Received 3 August 2022; accepted 18 August 2022. Date of publication 31 August 2022; date of current version 28 September 2022.

Digital Object Identifier 10.1109/OJAP.2022.3203253

Combined Single-Layer K-Band Transmitarray and Beamforming S-Band Antenna Array for Satcom

DANIEL EDELGAARD SERUP, GERT FRØLUND PEDERSEN (Senior Member, IEEE), AND SHUAI ZHANG, (Senior Member, IEEE)

Antenna, Propagation and Millimeter-Wave Section, Department of Electronic Systems, Aalborg University, 9220 Aalborg, Denmark

CORRESPONDING AUTHOR: S. ZHANG (e-mail: sz@es.aau.dk)

This work was supported by the InnovationsFonden Project of MARS2.

ABSTRACT In this paper, a dual-band antenna at 4.5 GHz and 25 GHz is presented. The antenna is a low-frequency phased patch antenna array combined with a high-frequency transmitarray with a fixed beam. The low-frequency patch antenna array and the high-frequency transmitarray feed share the same aperture area. The high-frequency transmitarray surface only uses a single substrate layer and is electrically transparent to the low-frequency phased array with beamforming. The antenna is measured to achieve an impedance bandwidth of 350 MHz and 3 GHz, and a gain of 15.4 dBi and 23.5 dBi, at S- and K-band respectively. With an impressive frequency-ratio of 5.55 and an aperture area of only 12x12cm the antenna achieves an aperture efficiency of 66% and 15% in the two bands respectively. Additionally, the low-frequency beamforming capabilities (with the existence of transmitarray surface) are measured and the antenna is shown to have a 60-degree scanning range with only a 0.22 dB gain drop-off.

INDEX TERMS Dual-band, S-band, K-band, antenna, transmitarray, antenna array, beamforming, satellite, nano-satellite, shared aperture, prototype, measurement.

I. INTRODUCTION

ANTENNAS can be designed with different features and advantages. Some features and benefits come at the expense of reduced antenna performance in another area. Different use-cases and applications set different requirements for the performance of the antenna [1], [2], [3], [4], [5], [6], [7], [8].

For this work, a very specific use-case is considered. The antenna should utilize commonly used satellite frequency bands. Thus, dual S- and K-band frequency operation is chosen. The antenna should have low-frequency beamforming capabilities while simultaneously maintaining a sufficient high-frequency gain. The purpose of these requirements is for the antenna to be used in a nano-satellite constellation. The high-frequency band is used to establish a high-speed connection to neighboring satellites in the constellation. The low-frequency antenna will utilize beamforming to maintain a communication link with Earth. Reflectarray and transmitarray antennas are often reported in the literature to yield a high gain [9], [10], [11], [12], [13], [14], [15], [16], [17], [18], [19], [20], [21], [22], [23], [24], [25], [26], [27], [28]. For space applications, multi-part antennas such as reflectarray and transmitarray antennas often require a deployment mechanism. Between the two options, a transmitarray might be the better option, as the feeding source could be installed on the stationary part of the antenna. The installation of the antenna unto a satellite is a complex and very application-specific task. The antenna is envisioned to be installed on one of then sides of the satellite. No further discussion about antenna installation will be conducted. None of the antennas reported in the state-of-the-art literature have shown the desired antenna performance characteristics of both simultaneously having dual-band operation with a high frequency-ration and low-frequency beamforming capabilities. Some antennas reported in the literature satisfies parts of the requirements, but unlike the antenna presented in this paper none of them covers all the listed requirements simultaneously [16], [18], [22], [24].

In [16] a dual-band transmitarray is presented. However, it is designed for k- and ka-band and could not easily be scaled to a larger frequency-ratio. The antenna presented in [18] is a dual-band antenna that has the same issue. Its

frequency-ratio is very low as it is designed for two k-band frequencies. Neither the antenna from [16] nor [18] have any beamforming capabilities. In [22] a dual-band antenna with beam-steering is presented. Ignoring the low frequency-ratio the antenna still has some disadvantages. To beam-steer, the transmission surface has to be physically moved. But, since the surface also contains the unit elements for the other frequency band the beam-steering cannot be performed without affecting the opposite band negatively. Paper [24] presents a beam-steering method that used switched to realize a few predefined beam directions. Even with this single band antenna design realizing wide low loss scanning would be troublesome.

In this paper, an antenna design with the described features will be presented. The antenna is a dual S- & K-band antenna with low-frequency beamforming capabilities. Dual-band functionality is achieved by combining a low-frequency phased patch antenna array with a high-frequency transmitarray in the same aperture area. Compared with antennas reported in the state-of-the-art, the antenna of this paper is unique. It enables low-frequency beamforming with an dual-band antenna that has a very high frequency-ratio. It achieves this without significantly sacrificing the radiation performance in either of the two bands. To realize good low-frequency beamforming performance the high-frequency transmitarray surface needs to be electrically transparent at the lower frequency. In this paper, good transparency is achieved with the designed single-layer transmitarray unit element.

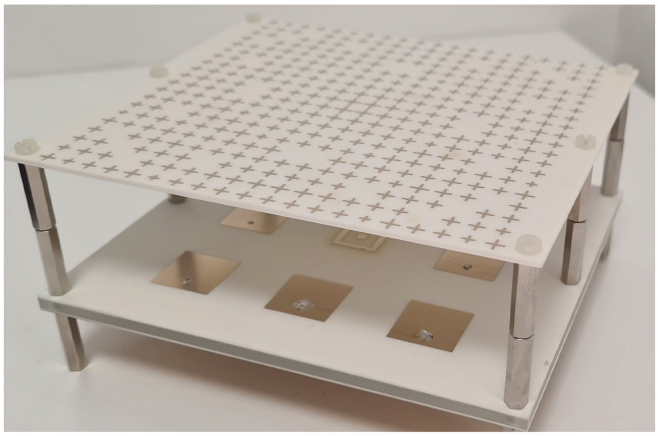

FIGURE 1. The fabricated antenna prototype.

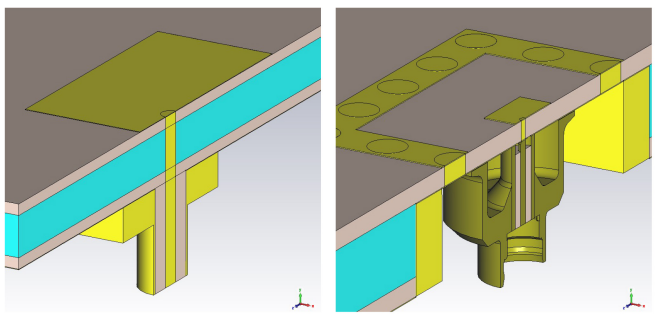

(a) (b)

FIGURE 2. Cross-section cut of the simulation model. (a) Low-frequency feed. (b) High-frequency feed.

II. ANTENNA CONFIGURATION

The fabricated antenna prototype is seen in Fig. 1. The proposed antenna has two parts made with a total of four different layers. The bottom part consists of a single 3 mm thick layer of Polypropylene (PP) material placed between two Rogers RO4003C layers both with a thickness of 0.812 mm. The top part is a single layer of RO4003 with a thickness of 1.524 mm. The substrate layers have a permittivity of 3.55, and a loss tangent of 0.027. The PP material has a permittivity of 2.245 and a loss tangent of 0.002. All layers have the same size. The high-frequency unit elements are contained within a 120x120 mm area but the layers have been enlarged by 8 mm on the two opposite sides of the board to allow for six metal mounting beams to be installed. The purpose of the metal beams is to mechanically hold the top surface securely and centered above the lower part. The separation between the two parts is 40 mm.

The bottom part houses the low-frequency patch antenna array and the high-frequency transmitarray feed. The top part houses the high-frequency transmitarray surface. The low-frequency patch antenna array has eight elements in a 3-by-3 configuration with the center element missing. The center element is removed to accommodate the high-frequency transmitarray feed. The low-frequency patch antenna elements has a center-to-center separation of 35 mm. This distance is calculated using $d = \frac{\lambda}{1 + sin(\theta)}$. The selected distance aims at a scanning range of $\pm 60^{\circ}$ without grating lobes.

Fig. 2 shows two cross-section pictures of the bottom part of the proposed antenna. Fig. 2(a) shows the feed of the low-frequency part. The low-frequency patch antenna elements are 17.75 mm. They are fed with SMA type connectors from the bottom of the three layers. The connector pins pass through a 4.15 mm opening in the ground plane and are soldered to the patches 4.80 mm from the patch center Fig. 2(b) shows the feed of the high-frequency part. The high-frequency feed antenna element is 2.75 mm. It is fed with an MMPX type connector from the bottom of the topmost of the three layers. The connector is soldered to a circular pad with a diameter of 0.6 mm. A VIA that passes through a 1.25 mm opening in the ground plane connects the pad to the patches 0.75 mm from the patch center. Around the high-frequency patch, a grounded wall with 16 VIAs is used to shield the patch antenna from surface waves. The bottom two layers have a square cutaway with a size of 18 mm. In the cut-away, an aluminum grounded guard with a 2 mm thickness is inserted to ensure a connected and continuous ground for the high-frequency feed.

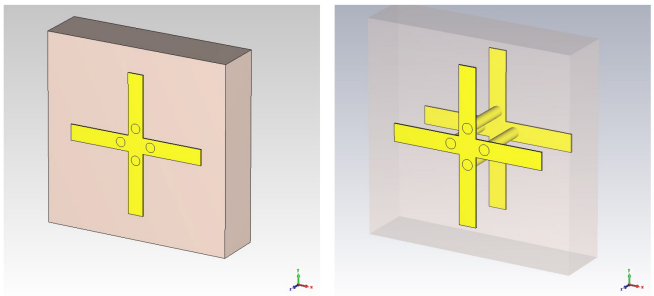

(a) (b)

FIGURE 3. Simulation model of the high-frequency transmitarray unit element. (a) Top view. (b) Model with the substrate layer partly transparent.

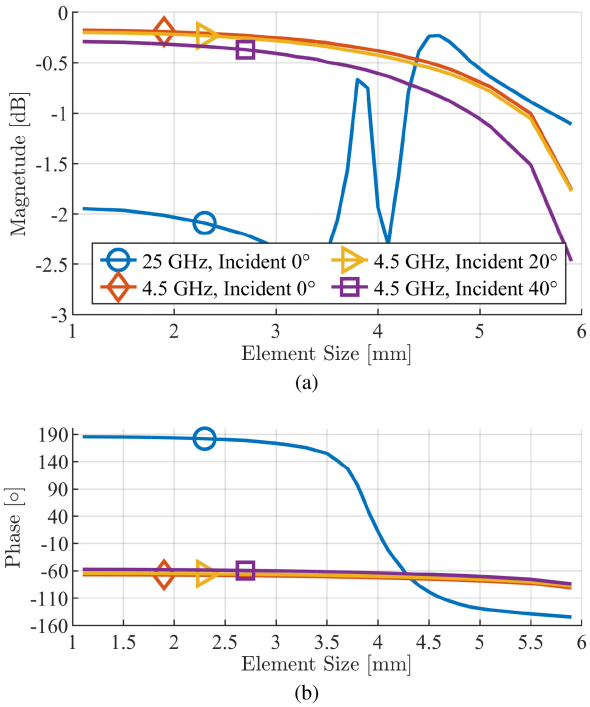

FIGURE 4. Simulated performance of the designed unit element. (a) Magnitude response. (b) Phase response.

The top layer houses a large number of high-frequency unit elements for the high-frequency transmitarray surface. Fig. 3 shows the simulation model of the high-frequency transmitarray unit cell. Each unit element is a copper plus shape that is printed on both sides of the substrate. The pluses on the two opposite sides are connected with four pins. The four pins increase the coupling between the plus-shapes which reduces the transmission loss. The pins all have a diameter of 0.3 mm and they are placed symmetrically in the plus shape 0.5 mm from the center of the plus shapes. The desired phase distribution is generated by tuning the length of the plus-shaped unit elements in the range from 1.3 mm to 5.9 mm. The elements are arranged in a square grid with a 6 mm spacing.

Fig. 4 shows the simulated phase and magnitude response of the unit element at the two center frequencies for different

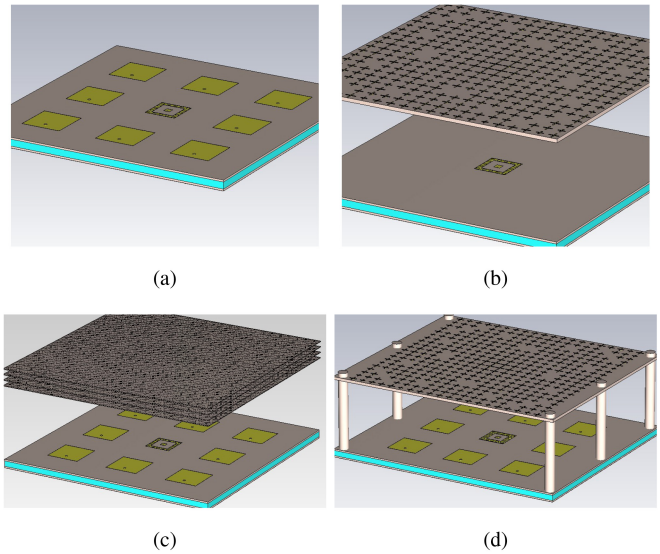

(a) (b) (c) (d)

FIGURE 5. Simulation model of the reference antennas used to evaluate the performance of the proposed antenna. (a) Low-frequency only reference (LF Ref.). (b) High-frequency only reference (HF Ref.). (c) Multi-layer transmitarray reference (ML Ref.). (d) Simulation model of the prototype antenna (Prot. Sim.).

element sizes and incident angles. The unit element is designed to have a low loss and Fig. 4(a) shows that the unit element has a loss of less than 2.5 dB for both frequency bands. Even for different low-frequency incident angles, the loss remains low. As seen from Fig. 4(b) the unit element achieves a phase range of 330° at 25 GHz. Additionally, for different incident angles at a frequency of 4.5 GHz the unit element has a maximum phase shift of 7°.

III. ANTENNA PROTOTYPE MEASUREMENT AND EVALUATION

Fig. 1 shows the fabricated prototype antenna. In this section, the measured performance of the antenna prototype will be presented in a comparison with four simulated antennas. The simulated antennas used for the comparison are the antennas seen in Fig. 5.

The eight low-frequency antenna ports are measured individually in an anechoic chamber. While measuring one port the other ports are terminated in a matched load. After the measurement, MATLAB is used to compute a combined low-frequency radiation pattern. The combined radiation pattern is computed as the phased and weighted superposition of the eight individual radiation pattern measurements.

A comparison between the measured and simulated low-frequency impedance match of the prototype antenna is seen in Fig. 6. It is seen that the fabricated prototype is shifted in frequency but still maintains a wide impedance bandwidth of 350 MHz. The shift is likely caused by a slight discrepancy in the dialectic constant of the substrate material.

Fig. 7 shows the boresight realized gain of the low-frequency band. Fig. 8 shows the theta slice of the radiation pattern when beamforming with the low-frequency antenna part. Both figures are a comparison between the measured performance of the antenna prototype antenna and

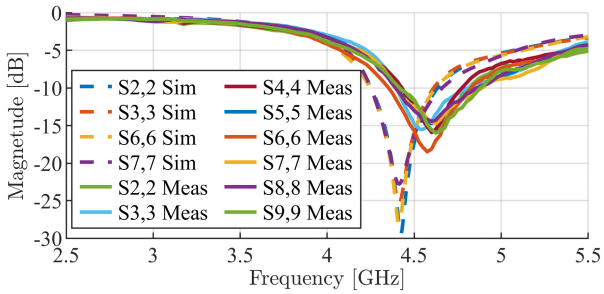

FIGURE 6. Measured and simulated low-frequency S-parameters of the prototype antenna.

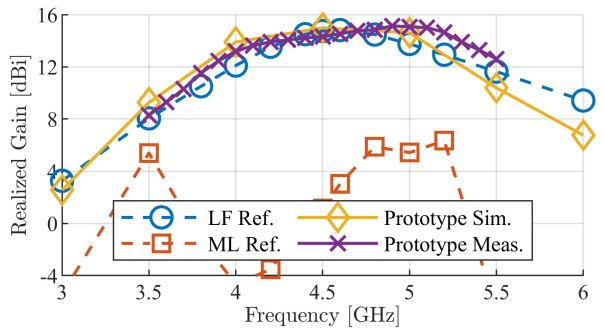

FIGURE 7. Measured and simulated low-frequency boresight realized gain of the prototype antenna.

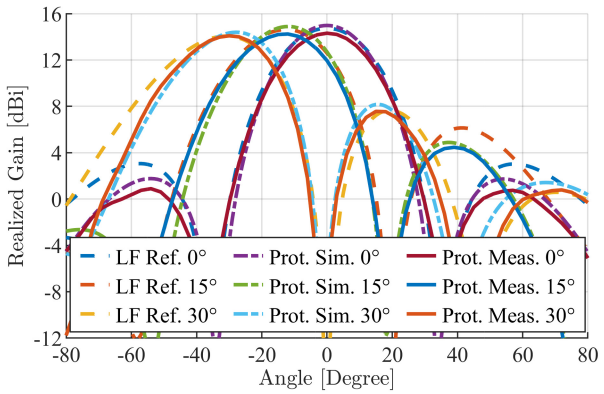

FIGURE 8. Measured and simulated low-frequency beamforming performance of the prototype antenna at 4.5 GHz.

the simulated performance of the reference antennas seen in Fig. 5.

In Fig. 7 it is seen that the reference antenna with a multi-layer transmitarray surface is significantly worse than the proposed antenna. This supports the claim that the designed single-layer unit element is more transparent at lower frequencies such as 4.5 GHz than the multi-layered unit elements typically found in the literature. The frequency-dependent gain response seen in Fig. 7 shows that the measurement is well-matched with the simulation.

Fig. 8 shows the measured and simulated low-frequency beamforming performance of the prototype antenna in comparison with the reference antenna seen in Fig. 5(a). Because of the good low-frequency transparency of the

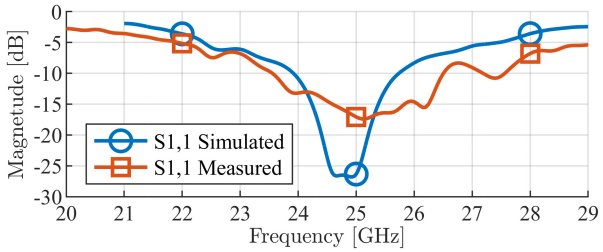

FIGURE 9. Measured and simulated high-frequency S-parameters of the prototype antenna.

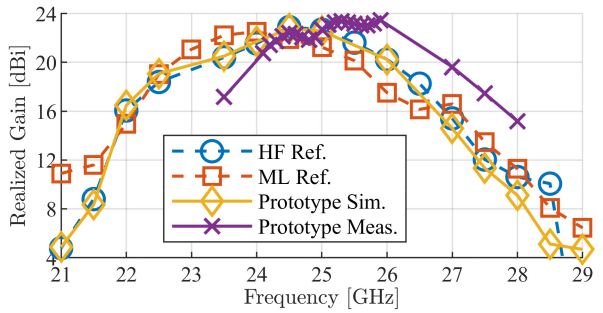

FIGURE 10. Measured and simulated high-frequency boresight realized gain of the prototype antenna.

designed transmitarray unit elements, the beamforming performance of the low-frequency antenna part is not negatively affected by the presence of the high-frequency transmitarray surface. The 60-degree scanning range gain drop-off is measured at only 0.22 dB for the antenna prototype.

Both Fig. 7 and Fig. 8 show that the gain of the measured antenna is very similar to the gain of both the simulated prototype and low-frequency only reference antenna. Thus it is concluded that the presence of the proposed transmitarray surface has no negative impact on the low-frequency gain characteristics.

A comparison between the measured and simulated high-frequency S1,1-Parameter of the prototype antenna is seen in Fig. 9. The impedance match of the fabricated prototype exceeds the expectation from the simulations, as the impedance bandwidth is more than 3 GHz.

Fig. 10 shows the boresight realized gain of the high-frequency band. The figure is a comparison between the measured performance of the antenna prototype antenna and the simulated performance of the reference antennas seen in Fig. 5. Since the figure shows that all the simulation curves are almost identical it is concluded that the addition of the low-frequency antenna elements does not negatively affect the performance of the high-frequency antenna part. And, that the designed single-layer unit element type is on par with the multi-layered element type. When comparing the curve of the simulated and the measured antenna prototype it is seen that the measured frequency-dependent gain seems to be slightly shifted to a higher frequency. This is consistent with the observations from the S-parameter measurements.

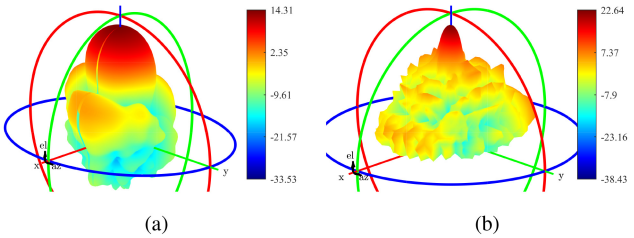

FIGURE 11. Measured radiation pattern. (a) Low-frequency mode at 4.5 GHz. (b) High-frequency mode at 25 GHz.

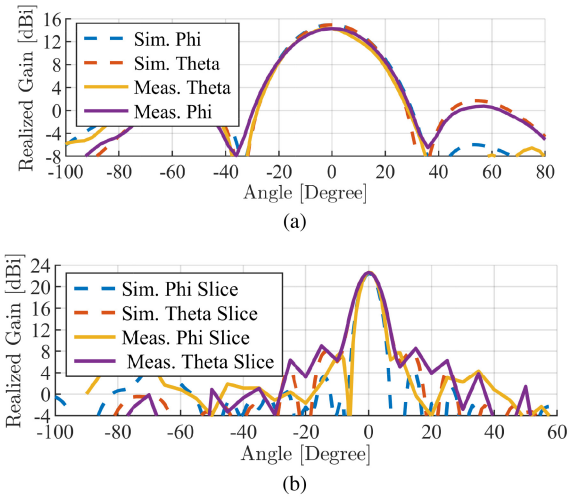

FIGURE 12. Simulated and measured radiation pattern slices. (a) Low-frequency mode at 4.5 GHz. (b) High-frequency mode at 25 GHz.

The overall measured gain is observed to be slightly higher in the measurement compared with the simulations.

Both the low-frequency and the high-frequency gain curves show a very similar frequency shift. Additionally, the S-parameters of both the low-/ and high-frequency parts of the prototype antenna also indicate a slight frequency shift. The consistency of the frequency shift further indicates that it might be caused by a slight discrepancy in the dialectic constant of the substrate. Because of the frequency shift, the high-frequency part of the antenna can be observed to achieve a slightly higher overall gain in Fig. 10. This higher gain is caused by the fact that the gain of the feeding horn is slightly increasing with frequency.

Fig. 11 and Fig. 12 shows the measured radiation pattern of the prototype antenna. The measured gain and radiation pattern shape are in very good agreement with the expectation from the simulation. Fig. 11(a) and 12(a) shows that low-frequency antenna part is able to achieve a realized gain of 14.31 dBi at 4.5 GHz. Fig. 11(b) and Fig. 12(b) shows that the transmitarray part of the prototype antenna achieves a realized gain of 22.64 dBi at 25 GHz.

The mutual and inner element coupling was not measured. However, Fig. 13 shows how the antenna prototype is simulated to have a low coupling between the two frequency

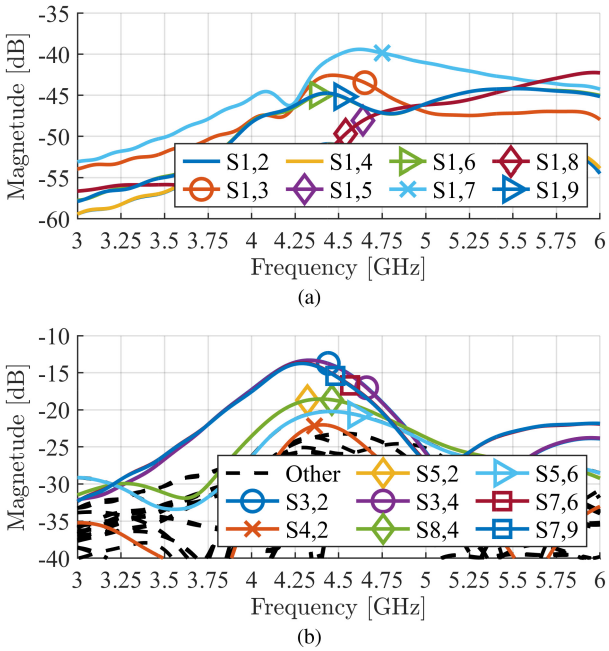

FIGURE 13. Simulated low-frequency S-parameters of the proposed antenna. (a) Mutual-coupling. (b) Low- to high-frequency coupling.

TABLE 1. Performance comparison between the proposed antenna and other antennas found in the state-of-the-art literature.

Ant.	*CF [GHz]*	*FR [1]*	*SL [1]*	*AE [%]*	*BFC*
Center Frequency (CF), Frequency-Ratio (FR), Surface Layers (SL), Aperture Efficiency (AE), Beamforming Capable (BFC)					
This Work	4.5 & 25	5.55	1	66 & 15	Yes
[16]	19.5 & 29	1.49	2	23.6 & 21.3	No
[18]	19.8 & 29.1	1.47	4	20.0 & 18.1	No
[22]	20 & 30	1.50	2	13.6 & 9.3	Yes
[24]	28	-	3	23.4	Yes

bands of less than −38 dB and a mutual coupling between the low-frequency elements of less than −14 dB.

IV. STATE OF THE ART COMPARISON

Table 1 shows a compression between the antenna presented in this work and various other antennas reported in the state-of-the-art.

The proposed prototype antenna achieves dual-band operation with a high-frequency ratio and the antenna also achieves low-frequency beam-forming. The novelty of the antenna is that it achieves these two performance characteristics without significantly sacrificing the radiation performance in either of the two bands. The proposed antenna has a slightly lower high-frequency aperture efficiency, but the high-frequency radiation performance is still deemed to be very competitive.

V. CONCLUSION

A shared aperture dual-band transmitarray and patch antenna array for S- and K-band with beamforming capabilities has

been successfully designed. A prototype antenna is measured to have a high similarity to the simulated results. The measurement shows the antenna to achieve impedance bandwidths of 350 MHz and 3 GHz, and a realized gains of 14.31 dBi and 22.64 dBi, at 4.5 GHz and 25. GHz, respectively. Additionally, the prototype antenna is shown to only have a 0.22 dB gain drop-off in a 60-degree beam scanning range. The design and unique features of the presented antenna make it interesting for many new and different use-cases and applications including satellite communication.

REFERENCES

[1] T. Li and Z. N. Chen, "Shared-surface dual-band antenna for 5G applications," *IEEE Trans. Antennas Propag.*, vol. 68, no. 2, pp. 1128–1133, Feb. 2020.

[2] F. Qin *et al.*, "A simple low-cost shared-aperture dual-band dual-polarized high-gain antenna for synthetic aperture radars," *IEEE Trans. Antennas Propag.*, vol. 64, no. 7, pp. 2914–2922, Jul. 2016.

[3] A. I. Sandhu, E. Arnieri, G. Amendola, L. Boccia, E. Meniconi, and V. Ziegler, "Radiating elements for shared aperture Tx/Rx phased arrays at K/Ka band," *IEEE Trans. Antennas Propag.*, vol. 64, no. 6, pp. 2270–2282, Jun. 2016.

[4] C. Mao, S. Gao, Y. Wang, Q. Chu, and X. Yang, "Dual-band circularly polarized shared-aperture array for *C*-/*X*-band satellite communications," *IEEE Trans. Antennas Propag.*, vol. 65, no. 10, pp. 5171–5178, Oct. 2017.

[5] D. E. Serup, R. J. Williams, S. Zhang, and G. F. Pedersen, "Shared aperture dual S- and X-band antenna for nano-satellite applications," in *Proc. 14th Eur. Conf. Antennas Propag. (EuCAP)*, 2020, pp. 1–9.

[6] D. E. Serup, R. J. Williams, S. Zhang, and G. F. Pedersen, "Dual S- and X-band shared aperture antenna for nano-satellite applications," in *Proc. 15th Eur. Conf. Antennas Propag. (EuCAP)*, 2021, pp. 1–9.

[7] D. E. Serup, S. Zhang, and G. F. Pedersen, "Single feed multi-resonant connected metasurface antenna for nano-satellite applications," in *Proc. 15th Eur. Conf. Antennas Propag. (EuCAP)*, 2021, pp. 1–5.

[8] P. Mei, S. Zhang, and G. F. Pedersen, "A dual-polarized and high-gain X-/Ka-band shared-aperture antenna with high aperture reuse efficiency," *IEEE Trans. Antennas Propag.*, vol. 69, no. 3, pp. 1334–1344, Mar. 2021.

[9] L. Guo, P. Tan, and T. Chio, "Single-layered broadband dual-band reflectarray with linear orthogonal polarizations," *IEEE Trans. Antennas Propag.*, vol. 64, no. 9, pp. 4064–4068, Sep. 2016.

[10] T. Smith, U. Gothelf, O. S. Kim, and O. Breinbjerg, "An FSS-backed 20/30 GHz circularly polarized reflectarray for a shared aperture L- and Ka-band satellite communication antenna," *IEEE Trans. Antennas Propag.*, vol. 62, no. 2, pp. 661–668, Feb. 2014.

[11] R. Deng, F. Yang, S. Xu, and M. Li, "An FSS-backed 20/30-GHz dual-band circularly polarized reflectarray with suppressed mutual coupling and enhanced performance," *IEEE Trans. Antennas Propag.*, vol. 65, no. 2, pp. 926–931, Feb. 2017.

[12] C. Han, J. Huang, and K. Chang, "A high efficiency offset-fed X/ka-dual-band reflectarray using thin membranes," *IEEE Trans. Antennas Propag.*, vol. 53, no. 9, pp. 2792–2798, Sep. 2005.

[13] Y. Chen, L. Chen, H. Wang, X. Gu, and X. Shi, "Dual-band crossed-dipole reflectarray with dual-band frequency selective surface," *IEEE Antennas Wireless Propag. Lett.*, vol. 12, pp. 1157–1160, 2013.

[14] R. S. Malfajani and B. A. Arand, "Dual-band orthogonally polarized single-layer reflectarray antenna," *IEEE Trans. Antennas Propag.*, vol. 65, no. 11, pp. 6145–6150, Nov. 2017.

[15] D. E. Serup, G. F. Pedersen, and S. Zhang, "Dual-band shared aperture reflectarray and patch antenna array for S- and Ka-band," *IEEE Trans. Antennas Propag.*, vol. 70, no. 3, pp. 2340–2345, Mar. 2022.

[16] K. Pham, R. Sauleau, E. Fourn, F. Diaby, A. Clemente, and L. Dussopt, "K/Ka-band transmitarray antennas based on polarization twisted unit-cells," in *Proc. 12th Eur. Conf. Antennas Propag. (EuCAP)*, 2018, pp. 1–6.

[17] Z. Zhang, X. Li, C. Sun, Y. Liu, and G. Han, "Dual-band focused transmitarray antenna for microwave measurements," *IEEE Access*, vol. 8, pp. 100337–100345, 2020.

[18] R. Madi, A. Clemente, and R. Sauleau, "Dual-band dual-linearly polarized transmitarray at ka-band," in *Proc. 50th Eur. Microwave Conf. (EuMC)*, 2021, pp. 340–343.

[19] Q. Luo, S. Gao, M. Sobhy, and X. Yang, "Wideband transmitarray with reduced profile," *IEEE Antennas Wireless Propag. Lett.*, vol. 17, no. 3, pp. 450–453, Mar. 2018.

[20] X. Yi, T. Su, B. Wu, J. Chen, L. Yang, and X. Li, "A double-layer highly efficient and wideband transmitarray antenna," *IEEE Access*, vol. 7, pp. 23285–23290, 2019.

[21] Q. Luo *et al.*, "A hybrid design method for thin-panel transmitarray antennas," *IEEE Trans. Antennas Propag.*, vol. 67, no. 10, pp. 6473–6483, Oct. 2019.

[22] P. Naseri, S. A. Matos, J. R. Costa, C. A. Fernandes, and N. J. G. Fonseca, "Dual-band dual-linear-to-circular polarization converter in transmission mode application to *K*/*Ka*-band satellite communications," *IEEE Trans. Antennas Propag.*, vol. 66, no. 12, pp. 7128–7137, Dec. 2018.

[23] P.-Y. Feng, S.-W. Qu, X.-H. Chen, and S. Yang, "Low-profile high-gain and wide-angle beam scanning phased transmitarray antennas," *IEEE Access*, vol. 8, pp. 34276–34285, 2020.

[24] M. Jiang, Z. N. Chen, Y. Zhang, W. Hong, and X. Xuan, "Metamaterial-based thin planar lens antenna for spatial beamforming and multibeam massive MIMO," *IEEE Trans. Antennas Propag.*, vol. 65, no. 2, pp. 464–472, Feb. 2017.

[25] F. Diaby, A. Clemente, R. Sauleau, K. T. Pham, and L. Dussopt, "2 bit reconfigurable unit-cell and electronically steerable transmitarray at *Ka* -band," *IEEE Trans. Antennas Propag.*, vol. 68, no. 6, pp. 5003–5008, Jun. 2020.

[26] Q. Zeng, Z. Xue, W. Ren, and W. Li, "Dual-band beam-scanning antenna using rotatable planar phase gradient transmitarrays," *IEEE Trans. Antennas Propag.*, vol. 68, no. 6, pp. 5021–5026, Jun. 2020.

[27] X. Li, X. Li, and L. Yang, "Single-layer dual-band wide band-ratio reflectarray with orthogonal linear polarization," *IEEE Access*, vol. 8, pp. 93586–93593, 2020.

[28] R. Deng, Y. Mao, S. Xu, and F. Yang, "A single-layer dual-band circularly polarized reflectarray with high aperture efficiency," *IEEE Trans. Antennas Propag.*, vol. 63, no. 7, pp. 3317–3320, Jul. 2015.

[29] V. K. Kothapudi and V. Kumar, "A 6-port two-dimensional 3×3 series-fed planar array antenna for dual-polarized X-band airborne synthetic aperture radar applications," *IEEE Access*, vol. 6, pp. 12001–12007, 2018.

[30] V. K. Kothapudi and V. Kumar, "A single layer S/X-band series-fed shared aperture antenna for SAR applications," *Progr. Electromagn. Res. C*, vol. 76, pp. 207–219, Mar. 2017.

DANIEL EDELGAARD SERUP was born in Randers, Denmark, in 1994. He received the B.S. degree in electronic and IT and the M.S. degree in wireless communication systems from Aalborg University in 2017 and 2019, respectively, where he is currently pursuing the Ph.D. degree with the Department of Electronic Systems, Antennas, Propagation and Millimetre-Wave Systems Section. His current research interests are novel multi-functional antenna designs for small satellite and 5G applications with a special focus on reflectarrays and transmitarrays.

GERT FRØLUND PEDERSEN (Senior Member, IEEE) was born in 1965. He received the B.Sc. and E.E. (Hons.) degrees in electrical engineering from the College of Technology in Dublin, Dublin Institute of Technology, Dublin, Ireland, in 1991, and the M.Sc. (E.E.) and Ph.D. degrees from Aalborg University, Aalborg, Denmark, in 1993 and 2003, respectively. He has also worked as a Consultant for developments of more than 100 antennas for mobile terminals, including the first internal antenna for mobile phones, in 1994, with lowest SAR, first internal triple-band antenna, in 1998, with low SAR and high TRP and TIS, and lately various multiantenna systems rated as the most efficient on the market. He has worked most of the time with joint university and industry projects and have received more than 21 M$ indirect research funding. Since 1993, he has been with Aalborg University, where he is currently a Full Professor, heading the Antennas, Propagation and Millimeter-Wave Systems Laboratory with 25 researchers. He is also the Head of the Doctoral School on Wireless Communication with some 40 Ph.D. students enrolled. He is currently the Project Leader of the RANGE Project with a total budget of over $8 M investigating high performance centimetre/millimeter-wave antennas for 5G mobile phones. He has been one of the pioneers in establishing over-the-air measurement systems. The measurement technique is now well established for mobile terminals with single antennas and he was chairing the various COST groups with liaison to 3GPP and CTIA for over-the-air test of MIMO terminals. He is currently involved in MIMO OTA measurement. He has published more than 500 peer reviewed papers, six books, 12 book chapters, and holds over 50 patents. His research interests include radio communication for mobile terminals, especially small antennas, diversity systems, propagation, and biological effects.

SHUAI ZHANG (Senior Member, IEEE) received the B.E. degree from the University of Electronic Science and Technology of China, Chengdu, China, in 2007, and the Ph.D. degree in electromagnetic engineering from the Royal Institute of Technology (KTH), Stockholm, Sweden, in 2013, where he was a Research Fellow. In April 2014, he joined Aalborg University, Aalborg, Denmark, where he is currently working as an Associate Professor and the Leader of the Antennas Group. In 2010, he was a Visiting Researcher with Lund University, Lund, Sweden, and in 2011, he was with Sony Mobile Communications AB, Lund. He was also an External Antenna Specialist with Bang & Olufsen, Aalborg, from 2016 to 2017. He has coauthored over 90 articles in well-reputed international journals and over 16 (U.S. or WO) patents. His current research interests include mm-wave antennas for cellular communications, biological effects, CubeSat antennas, massive MIMO antennas, wireless sensors, and RFID antennas.